Unidirectional bulk conduction and the anomalous temperature dependence of drift current under a trap-density gradient

Yukio Watanabe

Department of Physics, Kyushu University, Fukuoka, Fukuoka 812-8581, Japan
(Received 6 September 2009; revised manuscript received 10 April 2010; published 18 May 2010)

Nonlinear drift conduction under a trap-density gradient is mathematically formulated. Semianalytical and numerical solutions demonstrate bulk-induced unidirectional current flow, i.e., rectification. The present theory is in excellent agreement with various experimental *J-V* characteristics (*J*: current density and *V*: applied voltage). At low *V*, the *J-V* characteristics are ohmic and bidirectional. As the injection increases, the *J-V* characteristics become nonlinear and exhibit unidirectionality under proper conditions. The major requirements for a large unidirectionality are the trap-density gradient $G \gg 1$, an intermediate *V*, and not too large trap-filling factor Θ, which requires the presence of acceptorlike traps. The unidirectional *J-V* characteristics due to the difference in trap-filled-to-trap-free-limit voltage V_{TFL} for forward and reverse bias markedly resemble the standard rectification. In addition, the trap-density gradient yields a positive *T* dependence of resistance for a proper set of parameters, evident $J \propto V^{1.5}$ characteristics, and a photovoltaic effect. The present results suggest that bulk conduction under trap-density gradient explains fractions of resistance switching and rectification phenomena. The semianalytical solutions are verified by numerical solutions and comparison with experiments. In particular, semianalytical solutions for shallow-trap case excellently fit the experimental data by three parameters in practice: two scaling factors and *G*.

I. INTRODUCTION

Current conduction through high-resistive materials has been revealing new physics.[1] For example, the investigations of resistance switching, which is pursued for the resistance-random access memory,[2–23] have encountered various non-ideal rectifying current-density-voltage (*J-V*) characteristics. Because rectification is attributed to asymmetric interfaces such as metal-semiconductor contacts, the resistance switching is attributed to surface.[6,7] However, evidence that the origin is a bulk part is reported.[4,7,8,10,18] Solution of this controversy is a starting basis to uncover their mechanisms. Furthermore, a positive temperature coefficient of resistance[24] and rectification phenomena exhibiting bulk conduction properties are observed in compositionally graded ferroelectric films[25] and perovskite oxides.[15,21] In addition, the origin of nonlinear nonquadratic *J-V* characteristics often remains unidentified. The present paper aims to understand these issues from a unified view and proposes bulk-originated rectification.

Numerous *J-V* characteristics exhibiting rectification have been explained well by existing theories such as Schottky emission.[1] Nonideal rectifying *J-V* characteristics, which are inessential deviations from the standard theories, have also been observed:[26–28] For example, the *J-V* characteristics of a metal-semiconductor contact agree with Schottky emission theory under reverse bias but exhibit the space-charge-limited conduction (SCLC) under forward bias. Essential deviations are also observed: The *J-V* characteristics disagree with surface-limited processes at *either* bias polarity but agree with bulk-limited conduction processes *at both bias polarities*.[4,8] For example, the *J-V* characteristics agree with the Mott-Gurney law[29–31] under forward bias and Ohm's law under reverse bias. These characteristics are inexplicable by conventional models such as intermediate layers, high-field effects, double Schottky barriers, bipolar carrier injections, or degraded surface barriers and have been a long-standing puzzle.[4,7,8,15]

A clue can be the fact that when current carries free electrons/holes (carriers) whose density exceeds far the equilibrium density, nonequilibrium free carriers are injected into the material to enable the SCLC.[29–31] An intensive carrier injection can create traps,[5,18] and various mechanisms can yield graded distribution of traps (Fig. 1), i.e., "trap-density gradient" (Sec. II). The present paper shows that nonlinear bulk conduction under a trap-density gradient exhibit rectification and bulk-limited-conduction characteristics as well as a positive-temperature coefficient of resistance.

To formulate bulk conduction, we regard the SCLC (Refs. 30–44) as a generic macroscopic description of the electric-field-induced drift with a self-consistent solution of Poisson equation including the electric field due to the carriers. That is, provided assumptions (1)–(3) in Sec. III are satisfied, generalized SCLC is a universal description of macroscopic bulk conduction as opposed to microscopic descriptions of elementary processes such as Poole-Frenkel and hopping conduction.

The SCLC theories proposed so far and the existing bulk conduction processes yield the *J-V* characteristics that are bidirectional or symmetric with respect to the polarity of the applied voltage (*V*). However, SCLC may exhibit unidirectionality owing to nonlinearity, when bulk part possesses some asymmetries with special properties. Indeed, for a case obeying the Mott and Gurney law ($J \propto V^2$), Sworakowski showed that the conduction could be asymmetric under spatially asymmetrical trap distributions.[41] On the other hand, most of experimental nonideal rectifications exhibit the *J-V* characteristics of $J \propto V^m$ dependence with $m \approx 1.5$ or $m \gg 2$, which necessitates the present formulation for a general case, which explains both rectification and various *J-V* characteristics.
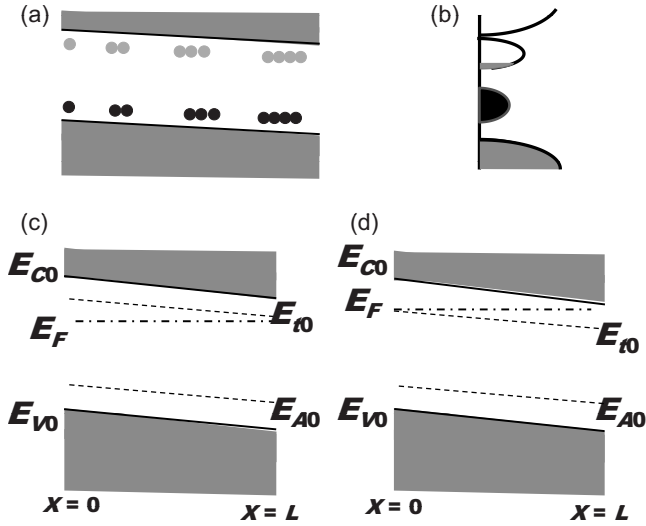
FIG. 1. (a) Trap distribution for trap-density gradient and (b) the corresponding band profile. Band diagrams for the initial state are shown for the (c) shallow-trap and (d) deep-trap case. The trap density N_t increases monotonically with x from $x=0$ to $x=L$. E_{C0}, E_{V0}, E_F, E_{t0}, and E_{A0} are the energy level of the conduction bottom edge and the valence-band top edge, the Fermi level, the energy level of the donor- and acceptor-type trap in the absence of the applied field, respectively.

In the present paper, we derive a set of differential equations for nonlinear conduction under a trap-density gradient considering rigorous carrier statistics. The theory presented below includes carrier statistics of the initial and injected state, which was neglected in the previous theory.[41] This carrier statistics yields a built-in potential, which is not the major origin of the unidirectional conduction but explains the photocurrent at zero-bias voltage. The present formulation can be regarded as that for diffusion-free drift conduction under a graded unipolar junction such as *nn* and *pp* junction (isotype homojunction with different doping density[1,45]). Approximate semianalytical and numerical solutions are presented. The unidirectionality predicted below is so evident that the resulting *J-V* characteristics can be mistakenly regarded as those of standard diodes.

The present theory excellently explains both *J-V* characteristics and rectification of various experiments, where the rectification originates from the bulk. In particular, the rectification in BiFeO$_3$ and SrTiO$_3$:Cr single crystals is attributed to the bulk.[4,8] In the present paper, the *J-V* characteristics of SrTiO$_3$:Cr single crystals exhibiting no hysteresis are carefully selected, because the comparison with the theory is only meaningful when the trap distribution is unchanged during the measurement. The subsequent part of the paper is organized as follows: origin of trap-density gradient (Sec. II), model and basic equations (Sec. III), semianalytical solutions (Sec. IV), asymptotic analytical solutions (Sec. V), self-consistent numerical solutions (Sec. VI), and comparison with experiments (Sec. VII).

II. ORIGIN OF GRADED DISTRIBUTION OF TRAPS

Typical mechanisms for trap-density gradient are carrier injection, oxygen vacancies, and epitaxial strain. Under high
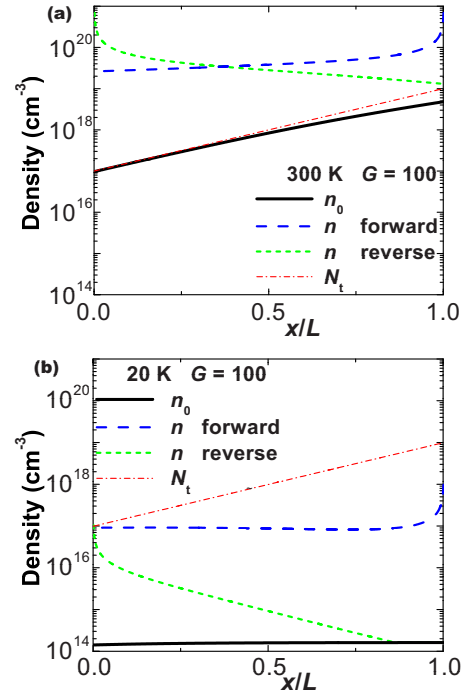

FIG. 2. (Color online) Theoretical free electron distributions for equilibrium state (n_0) and forward and reverse bias (n) for a given N_t (dashed-dotted lines), $N_A^-(x)=0.01N_t(x)$, $E_C-E_t=20$ meV, $N_{C0}=10^{19}$ cm^{-3} (300 K) and $J=10^3q^2\mu n_0^2(0)L/\varepsilon$. The solid, dashed, and short dashed lines correspond to n_0,n for forward and reverse bias, respectively.

electric field, nonequilibrium carries are injected from the electrodes and are observed to create traps or change trap distribution.[5,18,46–50] For example, SrTiO$_3$:Cr single crystals and thin films[8] become conductive by a forming process that involves a forced soft breakdown by a high electric field. The trap density increases with the number of these forming steps[18] and a trap-density gradient is directly confirmed.[9] Indeed, the resistance of most insulators degrades by forced current conduction under a high electric field,[47,50] which is attributed to the creation or migration of defects by impact ionization.[1,46,49,50]

The impact ionization is negligible under low electric field, which *allows us the assumption below that the trap density is unchanged during the measurements*. With increasing injection, traps are filled, and the conduction increases abruptly. Upon further increasing the electric field and injection, the impact ionization starts and then becomes an avalanche.[1] *The injection-induced traps are expected to decrease from one surface to the opposite surface because the injected carrier density or the field decreases from the surface of the injecting electrode to the opposite surface as shown by Mott-Gurney theory.*[31] Examples of such electron carrier distribution [$n(x)$] are seen in Fig. 2, where $n(x)$ is mostly due to injected electrons. Similarly, the field-induced migration of charged defects is expected to occur near the surface. In typical experiments, the applied voltage V increases from zero to the maximum ($V>0$) and then returns to zero, and often in addition, it decreases from zero to the minimum ($V<0$) and then returns to zero. This sequence

yields an asymmetrical trap distribution because the effect of the field is different before and after the sample becomes conductive.

The other representative mechanisms are chemical: oxygen vacancies and epitaxial strain. Volatile chemical species such as Pb, PbO, Bi, and BiO evaporate from the surface in vacuum or at a high temperature, which results in increase in vacancies towards the surface. The evaporation at the two surfaces is different owing to the temperature gradient and the materials in contact with the surfaces. Moreover, in vacuum-deposited thin films, vacancies are distributed asymmetrically between the top and bottom surfaces. Furthermore, the number of defects and dislocations changes from the bottom toward top surfaces, owing to the mechanical strain from the substrate. For these two mechanisms, the assumption used below that the trap density is unchanged during the measurements is satisfied even for a relatively high electric field. In addition, an intentionally formed trap-density gradient such as compositionally graded films is known.[25]

III. MODEL AND DERIVATION OF BASIC EQUATIONS

Figures 1(a) and 1(b) show the present model: a one-dimensional steady-state SCLC under a trap-density gradient of a total length L with coordinate x, where the trap density $N_t(x)$ increases monotonically with x. We employ assumption (7) below in addition to assumptions (1)–(6), which are frequently used in SCLC theories.[31] (1) Thermal energy is much lower than electrostatic energy and the diffusion current is neglected: $J = qn\mu\mathcal{E}$ [q: elementary charge, n: free electron carrier density, $\mu(>0)$: electron mobility, and $\mathcal{E}(x)$: applied field [$-dV(x)/dx$]]. (2) $\mathcal{E}(x)$ and the injection are not too high; thus, the initial trap distribution $N_t(x)$ is unchanged and no breakdown occurs. (3) The current carriers are electrons, which does not restrict the generality for unipolar conduction because of the electron-hole symmetry. (4) In-gap states near both contacts are abundant or the bulk part has a high resistance so that the effect of the potential barrier can be neglected and the contacts are regarded as injecting/ohmic contacts. (5) $\mathcal{E}(x)$ is not too high; thus, μ is independent of $\mathcal{E}(x)$. (6) The energy distribution of traps [Fig. 1(b)] is approximated by two types of traps [Fig. 1(a)]: donor-type traps and acceptors because the energy distribution profiles affect only the details of the J-V characteristics.[30] Here, donor-type traps are classified into shallow traps ($E_{t0} > E_F$) [Fig. 1(c)] and deep traps ($E_{t0} < E_F$) [Fig. 1(d)], where E_{t0}, and E_F are the energy level of the donor-type traps in the absence of an applied field, and the Fermi level, respectively. In addition, the acceptor-type traps with density N_A are assumed to be fully occupied, i.e., $N_A^- = N_A$. (7) The material is assumed to be uniform except for its trap density $N_t(x)$; the effective density of states of the conduction band N_C, the band gap E_g, and the value of $E_{t0}(x) - E_{C0}(x)$ are independent of x, where E_{C0} and E_{t0} are the energy level of the conduction-band edge and trap energy level in the absence of $\mathcal{E}(x)$, respectively [Figs. 1(c) and 1(d)].

The trap-density gradient creates a built-in potential $\phi_{bi}(x)$ (Ref. 1) and can be regarded as a series of *nn* junc-

tions. The carrier distribution under ϕ_{bi} and V can be deduced in the same manner as those in *pn* junctions (*p*: hole carrier): the standard theories of *pn* junction semiclassically treat electron. That is, free electron density is locally defined and is given by the integration of the occupied density of state from $E = E_{C0}(x)$ to $E = \infty$, where E_{C0} is the energy of a conduction-band electron.[1] The formula thus obtained is the same as Eq. (1a). This formulation is also applicable to the depletion region of the *pn* junction and, therefore, to the *nn* junction. Consequently, the standard expression for the free electron density in homogeneous semiconductors[1,31] is applicable to the present case. Therefore, in the absence of the applied field, free electron density [$n_0(x)$] is

$$n_0(x) = N_C \exp\left[-\frac{E_{C0}(x) - E_F}{k_B T}\right], \quad (1a)$$

where T and k_B are the ambient temperature and the Boltzmann constant, respectively. Similarly, the trapped carrier density in the absence of $\mathcal{E}(x)[n_{t0}(x)]$ is

$$n_{t0}(x) = N_t(x) \Big/ \left\{ 1 + g^{-1} \exp\left[\frac{E_{t0}(x) - E_F}{k_B T}\right] \right\}, \quad (1b)$$

where $N_t(x)$ and g are the concentration of shallow traps and the degeneracy factor, respectively. In the ideal diode equation by Shockley, the carrier density under the applied field $\mathcal{E}(x)$ is given by a formula similar to Eq. (1a) with the use of the quasi-Fermi level E_{Fn}. This formula is also applicable to the depletion region. Therefore, the carrier density $n(x)$ and trapped carrier density during injection $n_t(x)$ are

$$n(x) = N_C \exp\left[-\frac{E_C(x) - E_{Fn}}{k_B T}\right], \quad (1a')$$

$$n_t(x) = N_t(x) \Big/ \left\{ 1 + g^{-1} \exp\left[\frac{E_t(x) - E_{Fn}}{k_B T}\right] \right\}, \quad (1b')$$

where E_{Fn}, $E_C(x)$, and $E_t(x)$ are the quasi-Fermi level, the energy levels of the bottom edge of the conduction band and shallow trap under $\mathcal{E}(x)$, respectively. Equations (1a) and (1b) are the same as those used for the homogeneous case[1,31] except for the x dependence.

$E_{C0}(x)$, $E_{t0}(x)$, $E_C(x)$, and $E_t(x)$ are related to $\phi_{bi}(x)[\phi_{bi}(0) = 0]$ and the total electrostatic potential $V_T(x)$ by $E_{C0}(x) = E_{C0}(x=0) - q\phi_{bi}(x)$, $E_{t0}(x) = E_{t0}(x=0) - q\phi_{bi}(x)$, $E_C(x) = E_C(x=0) + qV_T(0) - qV_T(x)$, and $E_t(x) = E_t(x=0) + qV_T(0) - qV_T(x)$, and $V_T(x)$ is related to $V(x)$ by $V_T(x) = V(x) + \phi_{bi}(x)$. Therefore, $E_C(x) - E_t(x) = E_{C0}(x) - E_{t0}(x) = E_{C0}(0) - E_{t0}(0)$. The Poisson equations for $\phi_{bi}(x)$ and $V_T(x)$ are

$$\varepsilon \frac{d^2\phi_{bi}}{dx^2} = q[n_0(x) + N_A^-(x) - N_{t0}^+(x)], \quad (2a)$$

$$\varepsilon \frac{d^2 V_T}{dx^2} = q[n(x) + N_A^-(x) - N_t^+(x)],$$

where ε is the permittivity, and $N_{t0}^+(x)$ and $N_t^+(x)$ are the ionized trap density in the absence and the presence of the applied field $\mathcal{E}(x)$, respectively. In the previous study,[41] n_0,
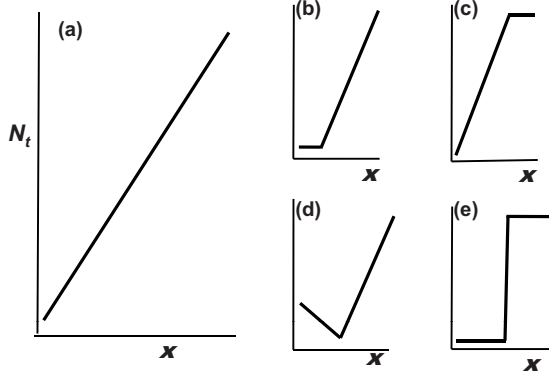
FIG. 3. Trap distribution types: (a) simple exponential distribution (the vertical axis is log scale) used in main results (Figs. 4–11). Appendices A and C discuss other variations: (b) exponential distribution with a low trap-density flat region, (c) exponential distribution with a high trap-density flat region, (d) valley type: combination of the type (a) and (e) abrupt step type.

n_{t0}, and the built-in potential were neglected. The subtraction of Eq. (2a) from the second equation [below Eq. (2a)] yields

$$\varepsilon \frac{d^2V}{dx^2} = q[n(x) + n_t(x) - n_0(x) - n_{t0}(x)], \quad (2b)$$

where we used the relationships $N_{t0}^+(x) = N_t(x) - n_{t0}(x)$ and $N_t^+(x) = N_t(x) - n_t(x)$.

For a given set of $N_t(x)$, $N_A(x)$, N_C, g, $E_{C0}(x=0) - E_{t0}(x=0)$, and T, Eqs. (1a), (1b), and (2a) are self-consistently solved to yield $n_0(x)$, $n_{t0}(x)$, and E_F. For a given $J(=qn\mu\mathcal{E})$, with these values (n_0, n_{t0}, and E_F) and the boundary conditions [$\mathcal{E}(L)=0$, $V(L)=0$ or $\mathcal{E}(0)=0$, $V(0)=0$], Eq. (2b) with Eqs. (1a) and (1b) yields $n(x)$, $n_t(x)$, and V, self-consistently. The spatial profile of $n_0(x)$, $n_{t0}(x)$, and $n(x)$ in Fig. 2 are calculated in this manner. Equation (2b) is the same as Eq. (4.2) of Ref. 31 derived for the homogeneous case except for the x dependence of n_0 and n_{t0}.

The J-V characteristics shown in Secs. V–VII *are for the trap distribution types shown in* Fig. 3(a) *with exponential N_t* distribution in which the vertical axis is log N_t. Similar results are found for another variation: linear N_t distribution. The J-V characteristics for Figs. 3(b)–3(e) are shown in Appendix A. The results are sorted by the trap-density gradient $G \equiv N_t(L)/N_t(0)$ and the trap filling factor $\Theta(x) \equiv n_0(x)/n_{t0}(x)$.[30,31] For $G=1$, the J-V characteristics presented below exactly agree with the previous studies.[31]

IV. SEMIANALYTICAL SOLUTIONS

Semianalytical solutions reduce the number of parameters and are useful for data fitting. Here, the conduction path L having a trap-density gradient is divided into $k_{\max}$ segments, and $N_t(x)$ and $N_A^-(x)$ are assumed to be constant in the kth segment [$N_t(x) = N_{t,k}$ and $N_A^-(x) = N_{A,k}^-$ for $(k-1)L/k_{\max} \le x < kL/k_{\max}$]. We denote the variables in the kth segment by the subscript k, in particular, $N_t(0) \equiv N_{t,1}$ and $N_t(L) \equiv N_{t,k \max}$ and define the exponential N_t distribution by a constant value of $N_{t,k}/N_{t,k-1}$.

We start with *shallow traps* that are assumed to remain shallow during injection and postulate $E_t - E_{Fn} > k_B T$. In this case, $\Theta(x)$ is constant (Θ_k) in the kth segment, which is derived similar to Eq. (2.18) of Ref. 31 ($\Theta_k \approx N/gN_{t,k}$, $N \equiv N_C \exp\{-[E_{C0}(0) - E_{t0}(0)]/k_B T\}$). Equation (2b) is rewritten as

$$\varepsilon \frac{d^2V}{dx^2} = q[n(x) - n_0(x)](1 + \Theta_k^{-1}). \quad (3)$$

We introduce two types of approximation for $n_0(x)$. Because electrons are distributed in equilibrium as a balance between the electrostatic force and the thermal diffusion, $n_0(x) = n_0$ (n_0: constant) is effective for $(E_C - E_t)/k_B T \gg 1$, which we call a constant-n_0 approximation (Appendix B). In the higher-order approximation, $n_0(x)$ is approximated as $n_0(x) = CN_t(x)$ (C: constant) for $(E_C - E_t)/k_B T < 1$, which we call an $n_0 \propto N_t$ approximation. Numerical solutions in Fig. 2, which yield self-consistent values of E_F, confirm the correctness of these approximations. For traps to be shallow, the condition $\Theta_k < 1$ requires $gN_t > N$ and a heavy compensation ($N_A^- \approx N_t$) (Appendix B).

Equation (3) is rewritten by the dimensionless quantities $u \equiv n_0(0)/n(x)$, $\eta_k \equiv N_{t,k}/N_{t,1}(\ge 1)$, $w \equiv x/L_*$, $W \equiv L/k_{\max}L_*$, $v = |V|/V_{bi2}$, $L_* \equiv L|J|/J_{bi2}$, and $j \equiv J/J_{bi2}$, where $V_{bi2} \equiv qn_0(0)L^2(1 + \Theta_1^{-1})/\varepsilon$ (twice the nominal built-in potential of the system), $J_{bi2} = q\mu n_0(0)V_{bi2}/L$ (nominal ohmic current induced by V_{bi2}), and $\Theta_1 = \Theta(0)$. By utilizing the solution for homogeneous cases in Ref. 31 and the continuity of $\mathcal{E}(x)$ and $V(x)$ at $x_k = (k-1)W$, we obtain the solution in the $n_0 \propto N_t$ approximation as the recurrence formulae

$$v_k = \frac{1}{r_k}\left[-\frac{u_k^2 - u_{k-1}^2}{2\eta_k} - \frac{u_k - u_{k-1}}{\eta_k^2} - \frac{\ln(|1 - \eta_k u_k|/|1 - \eta_k u_{k-1}|)}{\eta_k^3} \right] + v_{k-1} \quad (4)$$

$$-\frac{u_k - u_{k-1}}{\eta_k} - \frac{\ln(|1 - \eta_k u_k|/|1 - \eta_k u_{k-1}|)}{\eta_k^2} = r_k W, \quad (5)$$

where $u_k \equiv u(x_k)$ and $v_k \equiv v(x_k)$. For $\Theta_1 < 1$, the solutions are independent of Θ_1 and only depend on the gradient η_k, because $r_k \equiv (1 + \Theta_k^{-1})/(1 + \Theta_1^{-1})$ can be approximated as η_k. For a given J, free parameters for the shallow-trap case are G, $\Theta(0)(=\Theta_1)$, and the scaling factors V_{bi2} and J_{bi2}. We use $\Theta(0)$ as a representative value of $\Theta(x)$ below because $\Theta(x) < \Theta(0)$ for shallow traps owing to $\Theta_k \approx N/gN_{t,k}$.

For deep traps, Eq. (2b) is rewritten as $\varepsilon d^2V/d^2x = q[n(x) - N_t^+(x) - n_0(x) + N_{t0}^+(x)]$ because $n_{t0}(x) = N_t(x) - N_{t0}^+(x)$ and $n_t(x) = N_t(x) - N_t^+(x)$. For $E_F - E_t > k_B T$, Eqs. (1a) and (1b) yield $n_{t0}(x) \approx N_t(x)[1 - N/gn_0(x)]$ and $n_t(x) \approx N_t(x)[1 - N/gn(x)]$, and, therefore, $N_{t0}^+(x) = N_t(x)N/gn_0(x)$ and $N_t^+(x) = N_t(x)N/gn(x)$. By assuming the constancy of quantities in the kth segment, we obtain

$$\varepsilon \frac{d^2V}{dx^2} = q(n_k + A_k n_{0'k}^2/n_k - n_{0'k} - A_k n_{0,k}),$$

where $A_k \equiv N_{t0,k}^+/n_{0,k}$. By utilizing the solution for homogeneous cases in Ref. 31, we obtain the solution in the $n_0 \propto N_t$ approximation as the recurrence formulae for a given J,

TABLE I. Parameters used in the theories in addition to the normalization factors V_{bi2} and J_{bi2}. For a given J, V is calculated. C is a constant. For $\Theta(0) \ll 1$, semianalytical solutions for shallow traps are independent of $\Theta(0)$ and, therefore, $\Theta(0)$ is bracketed. For semianalytical solutions, one of three approximations is used: (shallow) $n_{0,k+1}/n_{0,k} = N_{t,k+1}/N_{t,k}$ (constant), (shallow) $n_{0,k} = n_0(0)$, (deep) $n_{0,k} = n_0(0)$ with $A_{k+1}/A_k = N_{t,k+1}/N_{t,k}$ (constant). In the most cases of numerical solutions, $N_t(0)(=10^{17}$ cm$^{-3})$ and $N_{C0}(=10^{19}$ cm$^{-3})$ are used, and always $g=1$, and two types of relationships of $N_A^-(x)$ and $N_t(x)$ are examined: $N_A^-(x) = \chi N_t(x)$ and $N_A^-(x) = \chi N_t(0)$.

Semianalytical (shallow)	$N_t(0)$, G, $C[=n_0(x)/N_t(x)]$ or $N_t(0)$, G, $n_0(0)$ $[\Theta(0)]$ $\{n_{0,k}, \Theta_{k+1}/\Theta_k, [\Theta(0)]\}$
Semianalytical (deep)	A_1, A_{k+1}/A_k, $n_0(0)$
Numerical [Eq. (2b)]	G, $E_{C0} - E_{t0}$, T, χ, $N_t(0)$, N_{C0}

$$v_k = \frac{1}{(1+A_k)\eta_k^3}\left[-(1+A_k^{-1})\eta_k(u_k - u_{k-1}) - \ln\left(\frac{|1-\eta_k u_k|}{|1-\eta_k u_{k-1}|} \right) \right.$$
$$\left. + \frac{1}{A_k^2}\ln\left(\frac{|1+A_k\eta_k u_k|}{|1+A_k\eta_k u_{k-1}|} \right) \right] + v_{k-1} \qquad (6)$$

$$\frac{1}{(1+A_k)\eta_k^2}\left[-\ln\left(\frac{|1-\eta_k u_k|}{|1-\eta_k u_{k-1}|} \right) - \frac{1}{A_k}\ln\left(\frac{|1+A_k\eta_k u_k|}{|1+A_k\eta_k u_{k-1}|} \right) \right]$$
$$= W, \qquad (7)$$

where $\eta_k = n_{0,k}/n_{0,1}$, $u_k = n_{0,k}/n(x)$, and $v = |V|/V_{bi2}$. $N_t(x)$ is specified by $N_t(0)$ and $G \equiv N_t(L)/N_t(0)$ (Table I). The solutions for shallow- and deep-trap cases in the constant-n_0 approximation are given by Eqs. (4)–(7) by setting $\eta_k = \eta_1$.

J-V characteristics under forward and reverse bias are calculated by Eqs. (4)–(7) in the limit $k_{max} = \infty$ and are shown in Figs. 4(a) and 4(b) for the shallow- and deep-trap cases, respectively. The $n_0 \propto N_t$ and constant-n_0 approximation are used for the shallow- and deep-trap case, respectively (Table I). However, *the $n_0 \propto N_t$ and constant-n_0 approximation yield essentially the same results* in both shallow and deep-trap case. Therefore, the major characteristics in Fig. 4 are of exact solutions, which is also confirmed by numerical solutions. The J-V characteristics are ohmic and bidirectional, i.e., nonrectifying for $v \ll 1$, i.e., $V \ll V_{bi2}$, of which mechanism is explained by Sec. V.

For shallow-trap cases [Fig. 4(a)], the $j \propto v^m$ dependence $(1 < m \le 2)$ and unidirectional J-V characteristics start to emerge at $v = 1 \sim G$. For $\Theta(0) < 1$, *rectification and J-V characteristics are found to be insensitive to $\Theta(0)$*. The direction of the electron flow for a forward bias is that of increasing N_t. The T dependence is represented by $\Theta(0)$, which increases with T. Equations (4) and (5) show that for $\Theta(0) \ge 1$ rectification diminishes with increasing $\Theta(0)$. In particular, for $v = \infty$, $r_k = 1$ in Eqs. (4) and (5), because $\Theta_k = \infty$ for $v = \infty$. In this case, Eqs. (4) and (5) show no rectification except for a negligibly small rectification near $v \sim 1$,
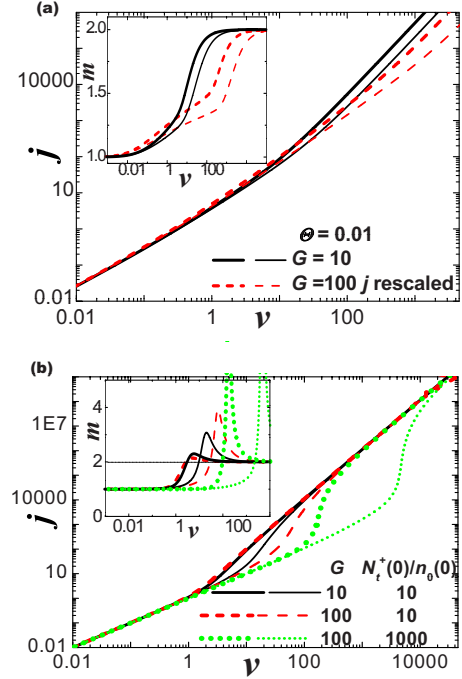

FIG. 4. (Color online) J-V characteristics of the forward-bias (thick lines) and reverse-bias (thin lines) branches for (a) shallow-trap and (b) deep-trap case by semianalytical solution in dimensionless quantities $v = |V|/V_{bi2}$ and $j \equiv |J|/J_{bi2}$, where $V_{bi2} \equiv qn_0(0)L^2[1 + \Theta^{-1}(0)]/\varepsilon$ and $J_{bi2} = q\mu n_0(0)V_{bi2}/L$. Insets show the v dependence of the exponent m in $j \propto v^m$. In (a) and (b) j for $G=100$ is rescaled so that the ohmic part for $G=100$ is aligned to that of $G=10$, and the original curve for $G=100$ is restored by division of 0.551. In (a), $\Theta(0)=0.01$. The J-V characteristics with $\Theta(0) < 0.01$ are almost overlapped with the present curves with the same G of (a) and those with $0.01 < \Theta(0) \le 1$ are similar to the present curves with the same G of (a). In all figures below, pairs of thick and thin line correspond to the forward- and reverse-bias curves.

which is consistent with asymptotic analytical results (Sec. V).

For deep-traps cases [Fig. 4(b)], the J-V characteristics consist of the $j \propto v$, the $j \propto v^m$ [$m > 2$; *trap-filled-to-trap-free-limit* (TFL) transition], and the $j \propto v^2$ region, where m increases with A. Rectification appears near the TFL voltage $V_{TFL} = (q/\varepsilon)\int_0^L dx \int_0^x dx N_t^+(x) \sim A_k V_{bi}(A_k \equiv N_{t0,k}^+/n_{0,k})$ and increases with G and A, which is due to the difference of V_{TFL} between the forward and reverse bias. This difference is explained by $V_{TFL} = (q/\varepsilon)\int_0^L dx \int_0^x dx N_t^+(x)$, which depends on the polarity of the applied field, because $N_t^+[x, \phi(x)]$ depends on the polarity of the applied field. The comparison of these results with experimental results requires caution, because a TFL transition often accompanies an irreversible change of the trap distribution, which appears as an *apparent* rectification and should be distinguished from the present theory. The direction of the electron flow for forward bias is that of decreasing N_t.

V. ASYMPTOTIC ANALYTICAL SOLUTIONS

This section shows the asymptotic solutions for $v \to 0$ and $v \to \infty$. For $v \to 0$, injection is negligible, which means that

$n(x) \approx n_0(x)$ and $n_t(x) \approx n_{t0}(x)$. Therefore, assumption (1) in Sec. III yields $J = qn_0(x)\mu\mathcal{E}$, which gives $V = -\int dx\mathcal{E} = R_0|J|$, where $R_0 = (q\mu)^{-1}\int dxn_0^{-1}(x)$ is independent of V and J. That is, the J-V characteristics are ohmic and show no rectification for $v \to 0$.

For $v \gg 1$, carriers are dominated by injected carriers [$n(x) \gg n_0(x)$ and $n_t(x) \gg n_{t0}(x)$], and Eq. (2b) reduces to $\varepsilon d^2V/dx^2 = qn(x)(1 + \Theta_*^{-1})$, where $\Theta_*(x) \equiv n(x)/n_t(x)$. Therefore, Eq. (2b) is rewritten as $-\varepsilon d^2V/dx^2 (dV/dx) = (J/\mu)(1 + \Theta_*^{-1})$, which yields $V = (2|J|/\varepsilon\mu)^{1/2}\int_0^L dx(\int_0^x dx1 + \Theta_*^{-1})^{1/2}$. Therefore, we obtain

$$|J| = \varepsilon\mu\frac{V^2}{2\Lambda^3}, \tag{8}$$

where $\Lambda \equiv [\int_0^L dx(\int_0^x dx1 + \Theta_*^{-1})^{1/2}]^{2/3}$ and for the opposite polarity, the integrations are performed from L to x and L to 0. Because Λ depends on the direction of the integration, the J-V characteristics depend on the polarity and show rectification in quadratic region, which is the Sworakowski's results.[41]

Equation (8) shows that the J-V characteristics at $v \gg 1$ are dominated by injection and insensitive to the details of $\Theta_*(x)$ and N_t distribution such as linear or exponential. For $v \to \infty$, we expect $n(x) \gg n_t(x)$, $n_0(x)$, $n_{t0}(x)$ and, therefore, $\Theta_* \gg 1$, for which Eq. (8) yields $J = 9\varepsilon|\mu|V^2/8L^3$. This condition of $n/n_t(=\Theta_*) \gg 1$ is realized for $N_C \gg$ maximum N_t, which seems satisfied in most cases. This disappearance of the rectification at $v \to \infty$ is confirmed by Fig. 5(a) and the semianalytical solutions for $\Theta \gg 1$.

The semianalytical and numerical results in Figs. 4–7 and Eqs. (4)–(7) agree with these asymptotic analytical results. Based on Eqs. (4) and (5), we examine the behavior of the shallow-trap case at $v \to \infty$, for which we have $u(\equiv n_0/n) \to 0$. In the lowest order of u, Eqs. (4) and (5) reduce to $w = (u_{k+1}^2 - u_0^2)/2$ and $v_{k+1} - v_k = (u_{k+1}^3 - u_k^3)/3$, and we have $L/L_* = k_{max}w = (u_{k\,max}^2 - u_0^2)/2$ and $v_{k\,max} - v_0 = (u_{k\,max}^3 - u_0^3)/3$. Because u_0 and v_0 are the ratio n_0/n and the normalized voltage at the injecting electrode, respectively, $u_0 = 0$ and $v_0 = 0$. Consequently, we have

$$v_{k\,max} = \frac{(2L/L_*)^{3/2}}{3},$$

which is rewritten as $J = 9\varepsilon\mu V^2/8L^3$ and shows no rectification. When Θ_* is constant (no trap-density gradient), Eq. (8) gives no rectification and the standard result $J = 9\varepsilon|\mu|V^2/8L^3(1 + \Theta_*^{-1})$, which is also derived from Eqs. (4) and (5).

VI. NUMERICAL SOLUTIONS

In realistic systems under a trap-density gradient, some traps may be shallow traps and others may be deep traps. These situations require study based on self-consistent solutions of Eq. (2a) with Eqs. (1a) and (1b) that yield $n_0(x)$ and $N_{t0}^+(x)$ (Fig. 2). The numerical results in Figs. 5–8 confirm the validity of the semianalytical solutions, especially for shallow-trap cases. N_A^- is introduced to represent the energy dispersion of traps, and two representative dispersions are
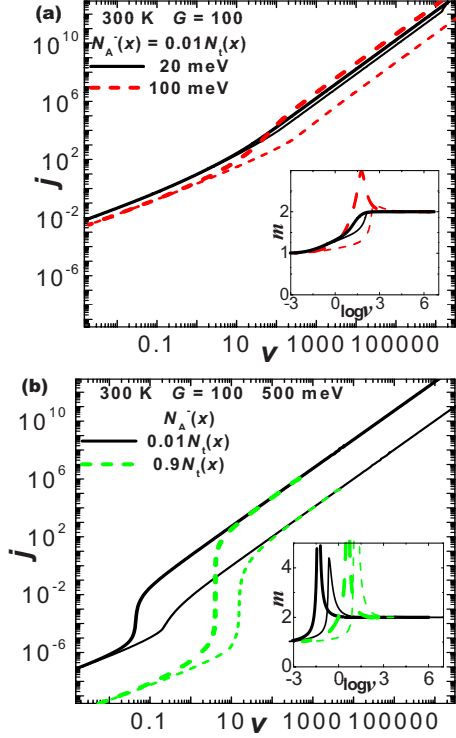

FIG. 5. (Color online) J-V characteristics of the forward- and reverse-bias branches by numerical solution. Insets show the v dependence of m in $j \propto v^m$. $E_C - E_t$ is 20 meV for the solid lines in (a), 100 meV for the dashed lines in (a), and 500 meV in (b). $N_A^-(x)$ is $0.01N_t(x)$ in (a), and $0.01N_t(x)$ (solid lines) and $0.9N_t(x)$ (dashed lines) in (b). $|J|$ and $|V|$ are normalized by $V_{bi2} = qN_t(0)L^2/\varepsilon$ and $J_{bi2} = q\mu N_t(0)V_{bi2}/L$, respectively. $[E_C(0) - E_F]/k_BT$, $\Theta(0)$, $\Theta(L)$, $A(0)$, and $A(L)$ of the solid and dashed lines are 3.9, 46, 0.94, 1.0, 1.0, and 1.1, 2.1, 0.15, 1.0, 1.1 in (a), and -4.6, 4.4×10^{-5}, 4.4×10^{-7}, 230, 2.3×10^4, and 2.2, 4.5×10^{-7}, 4.9×10^{-10}, 1.8×10^9, 1.8×10^9 in (b), respectively.

considered: (i) the energy dispersion is independent of x and (ii) the density of acceptorlike trap (N_A^-) is independent of the density of donorlike trap (N_t). In this two-level model, the dispersion type (i) and (ii) are represented by $N_A^-(x) = \chi N_t(x)$ and $N_A^-(x) = \chi N_t(0)$, respectively, where χ is a constant. Throughout this section, $g = 1$, $N_t(0) = 10^{17}$ cm^{-3}, $N_C = N_{C0}(T/300 \text{ K})^{3/2}$, and $N_{C0} = 10^{19}$ cm^{-3} (N_{C0}: effective density of states at 300 K).

A. J-V characteristics

In Fig. 5 ($T = 300$ K) and Fig. 6 ($T = 20$ K), the parameters of the initial state are $G = 100$, $E_{C0} - E_{t0}(=E_C - E_t)$, T, and $N_A^-(x)$ (Table I). The normalization factors V_{bi2} and J_{bi2} are $qN_t(0)L^2/\varepsilon$ and $q\mu N_t(0)V_{bi2}/L$, respectively, to show explicitly the dependence of the J-V characteristics on T and $E_{C0} - E_{t0}$. The values of $[E_{C0}(0) - E_F]/k_BT$, $\Theta(0)$ and so forth in captions are estimated from the self-consistently calculated $n_0(0)$ and $n_{t0}(0)$.

In Figs. 5 and 6, the J-V characteristics critically depend on $(E_{C0} - E_{t0})/k_BT$ but are relatively insensitive to χ and the dispersion types. Here, $(E_{C0} - E_{t0})/k_BT$ is the primary determinant of Θ and Θ decreases as $(E_{C0} - E_{t0})/k_BT$ increases.
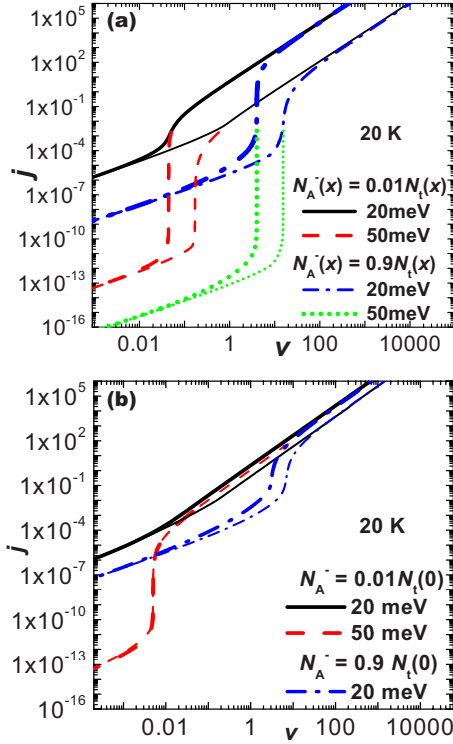
FIG. 6. (Color online) Same plots as Fig. 5 for 20 K. $N_A^-(x)$ $=\chi N_t(x)$ in (a) and $N_A^-(x)=\chi N_t(0)$ (b) with $\chi=0.01$ or 0.9. E_C-E_t $=20$ meV for the solid and dashed-dotted lines. $E_C-E_t=50$ meV for the dashed and dotted lines. In (a), $[E_C(0)-E_F]/k_BT$, $\Theta(0)$, $\Theta(L)$, $A(0)$, and $A(L)$ of the solid, dashed, dash-dot, and dotted lines are -4.5, 1.4×10^{-3}, 2.1×10^{-8}, 8.0, 4.8×10^5, and 2.2, 1.6×10^{-5}, 1.8×10^{-6}, 5.0×10^5, 5.0×10^7, and -4.6, 4.8×10^{-11}, 4.8×10^{-13}, 2.1×10^8, 2.1×10^{10}, and 2.2, 4.8×10^{-13}, 5.3×10^{-15}, 1.7×10^{13}, 1.8×10^{15}, respectively. In (b), those of the solid, dashed and dash-dot lines are -4.5, 1.4×10^{-3}, 3.6×10^{-4}, 7.9, 1.3, and 2.2, 1.5×10^{-4}, 2.0×10^{-6}, 5.0×10^4, 4.4×10^3, and -4.6, 4.8×10^{-11}, 4.8×10^{-11}, 2.1×10^8, 2.1×10^6, respectively.

An appreciable rectification exists for $\Theta\ll1$, especially for the dispersion type (i), and increases with G and Θ^{-1}, which is consistent with the semianalytical results. For $\Theta\ll1$, rectification at $v\gg1$ is almost independent of χ and $E_{C0}-E_{t0}$ owing to the insensitivity to Θ, as discussed in Sec. IV.

Shallow traps in the initial state are favored by a small $E_{C0}-E_{t0}$ and a large compensation, where the compensation is enhanced by a large χ and the dispersion type (i). The traps at $x=0$ are shallow for all the lines in Fig. 5(a), the dashed lines in Fig. 5(b), the dashed and dotted lines in Fig. 6(a), and the dashed lines in Fig. 6(b). In particular, the J-V characteristics in Fig. 5(a) closely resemble the semianalytical solutions in Fig. 4(a).

The curves for deep traps in Figs. 5(b), 6(a), and 6(b), which are for $(E_{C0}-E_{t0})/k_BT\gg1$ with $\chi\ll1$, are consistent with semianalytical results in Fig. 4(b). The increase in current at the TFL transition is sharper than that in Fig. 4(b), which is due to the extremely large A in Figs. 5(b) and 6(a). The trap-density gradient makes the threshold voltage of the TFL transition for forward bias different from that for reverse bias, which results in extremely large rectification. This rectification increases with G, $(E_{C0}-E_{t0})/k_BT$, and compen-
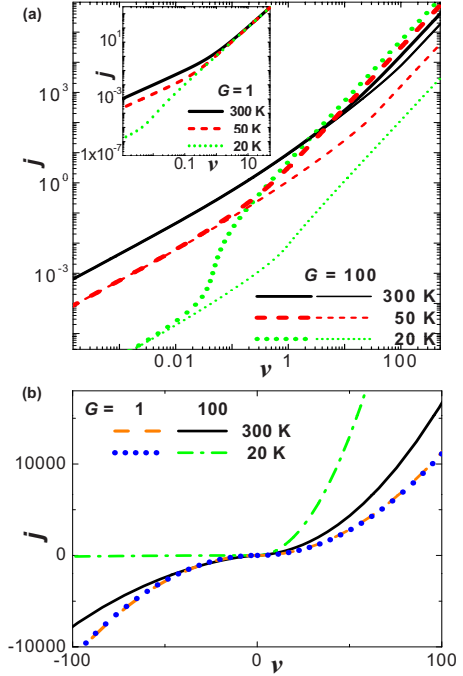

FIG. 7. (Color online) (a) Temperature dependence of J-V characteristics of the forward- and reverse-bias branches by numerical solutions with $E_C-E_t=20$ meV, $N_A^-(x)=0.01N_t(x)$ and $G=100$ with the normalization same as Fig. 5. (b) T dependence of J-V characteristics with ($G=100$) and without trap-density gradient ($G=1$): replot of J-V characteristics $\pm$ in (a). The curves with $G=1$ for T $=300$ and 20 K are completely overlapped.

sation (χ). The transition region exhibits $j\propto v^m$ with $m\geq2$, which yields a marked resemblance to the conventional surface-limited rectification.

The $j\propto v^{1.5}$ regions are evident, especially for a large χ or a large G, examples of which are in Figs. 8(b) and 8(e). All the curves in Fig. 5(a) and the solid lines in Fig. 6(b) correspond to shallow-trap cases [Fig. 4(a)] and exhibit the transition from an ohmic to $j\propto v^{1.5}$ with rectification, and then to $j\propto v^2$ with rectification. The J-V characteristics in the $j\propto v^2$ region are almost independent of E_C-E_t and T because of the dominance of injected electrons, whereas j in the $j\propto v^m$ ($m<2$) region critically depends on E_C-E_t and T. As shown in Sec. V, the J-V characteristics at $v\rightarrow\infty$ are bidirectional for $N_C\geq$ maximum N_t, example of which is the curves for $E_C-E_t=20$ meV of Fig. 5(a).

B. Temperature dependence

Because μ at low T is limited by the electrostatic scattering, μ is usually T independent at low T. Under this condition, standard SCLC with injecting ohmic contacts and G $=1$ is T independent for $v\gg1$, because n in $J=qn\mu\mathcal{E}$ is dominated by the injection, i.e., $n\gg n_0$, and is T independent. On the other hand, Figs. 7 and 8 show that the trap-density gradient induces an unconventional T dependence in proper ranges of v. The parameters in Figs. 7 and 8 are the same as those in Sec. VI A except for $E_C-E_t=20$ meV and those given below.
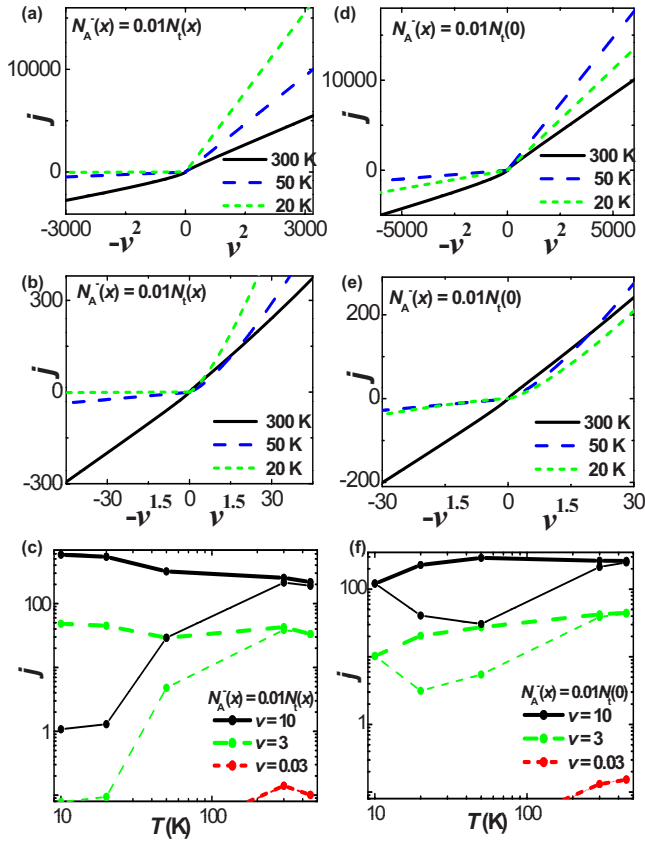
FIG. 8. (Color online) T dependence of J-V characteristics in j-v^2 [(a) and (d)] and j-$v^{1.5}$ plot [(b) and (e)] and T dependence of j at different v. $N_A^-(x) = 0.01 \, N_t(x)$ and $N_A^-(x) = 0.01 \, N_t(0)$ in (a)–(c) and (d)–(f), respectively. In (c) and (f), the thick and thin lines correspond to the forward and reverse characteristics, respectively, and the reverse characteristics for $v = 0.03$ are out of scale and are not shown.

FIG. 9. (Color online) Theoretical (solid lines) and experimental (open circle) J-V characteristics of Au/SrTiO$_3$:Cr single crystal/Au. (b) and (c) are replots of (a), and (e) and (f) are replots of (d). Two experimental data point at each V, which are overlapped, are those during increasing and decreasing V. The fitting parameters are $V_{bi2} = 1.2$ mV, $J_{bi2} = 0.82$ μA mm^{-2}, and $G = 100$ for (a)–(c) and $V_{bi2} = 110$ mV, $J_{bi2} = 0.23$ μA mm^{-2}, and $G = 1000$ for (d)–(f).

At $v \ll 1$ in Fig. 7(a), the conductance increases evidently with T, owing to the thermal activation of equilibrium free electrons (n_0). At $v > 1$ for $G = 1$, the conductance is independent of T, χ, and the trap distribution types [inset of Fig. 7(a)]. At $v \gg 1$ for $G > 1$, the conductance depends weakly on T, χ, and the trap distribution types. The trap-density gradient steepens the TFL transition for forward bias and slows it down for reverse bias. This steepening and slowing decrease with increasing T, which induces the decrease in forward bias current with T. Consequently, a positive-T coefficient of resistance (PTCR) emerges for forward bias [Fig. 7(a)], which is evident in linear-scale replots [Fig. 7(b)]. In addition, a v range exhibiting a PTCR exists also for a fixed $N_A^-(x)$, which however is less evident than for $N_A^-(x) \propto N_t(x)$ (Fig. 8).

The PTCR for $N_A^-(x) \propto N_t(x)$ appears in the $j \propto v^2$ region [Fig. 8(a)] and the $j \propto v^{1.5}$ region [Fig. 8(b)]. Similar results are found for a fixed $N_A^-(x)$ case [Figs. 8(d) and 8(e)]. The T dependence for the $N_A^-(x) \propto N_t(x)$ and fixed $N_A^-(x)$ cases is summarized in Figs. 8(c) and 8(f), respectively. In both figures, a PTCR appears for $v \gg 1$ under forward bias. A few differences exist between the $N_A^-(x) \propto N_t(x)$ and fixed $N_A^-(x)$ cases: For $N_A^-(x) \propto N_t(x)$, a PTCR appears for all v values [Fig. 8(c)]. For fixed $N_A^-(x)$ case, a PTCR appears at high T
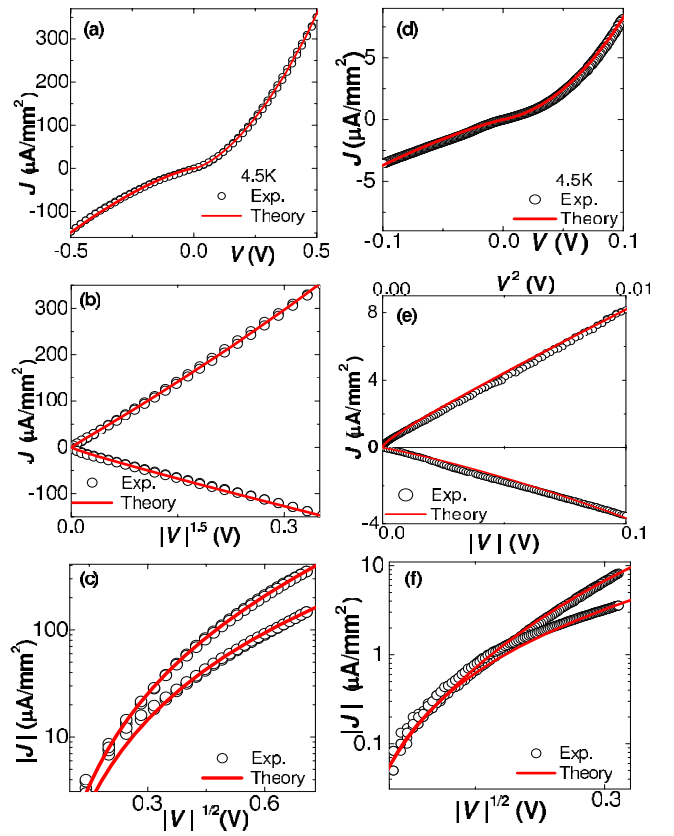
under forward bias above $v \approx 10$ and at low T under reverse bias [Fig. 8(f)]. These results show $j \propto v^2$ or $j \propto v^{1.5}$ with rectification and a PTCR under trap-density gradient, when N_A distribution, v and $(E_{C0} - E_{t0})/k_B T$ are proper and μ is T independent.

VII. COMPARISON WITH EXPERIMENTS

Experimental J-V characteristics of single crystals are compared with the present theory for shallow-trap (Fig. 9) and deep-trap cases (Fig. 10). The sample for Fig. 9 is a 10-μm-thick (001)-oriented SrTiO$_3$ single crystal with 0.2% Cr grown by the floating-zone melting and has a capacitor structure with Au electrodes on both surfaces. Details of the sample are described in Ref. 8. This crystal was initially highly insulating and became conductive upon repeated current injections by an electric field > 0.1 MV/cm. The experiments on SrTiO$_3$:Cr single crystals[5,11,18] show that traps or defects created by the injection thinned the Schottky barriers enough to be regarded as ohmic contacts.[1,30] In particular, the trap-density gradient is experimentally confirmed.[9] One of the J-V characteristics in high-resistance states after these treatments is shown in Fig. 9(a), and those in Fig. 9(d)
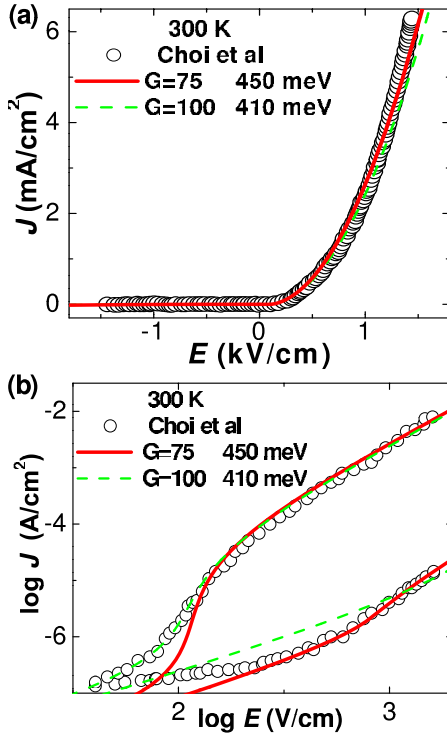
FIG. 10. (Color online) Comparison of the theoretical (solid lines) and experimental (open circles) J-V characteristics of Au electrode/BiFeO$_3$ single crystal/Au electrode at 300 K. The experimental are from supporting material of Ref. 4.

are measured before Fig. 9(a) and exposed to the injection less than the state of Fig. 9(a).

In Fig. 9, the trap distribution is expected to remain unchanged during the measurement of J-V characteristics because the maximum applied voltage and maximum current density are less than one tenth of those used to change the resistance. In Fig. 9, the J-V curves of the increasing and decreasing V overlap, and the J-V curves remain the same during repeated measurements. This proves that the trap distribution remained unchanged. In addition, the low temperature enables an acute detection of surface-limited conduction processes, if they exist. When rectification is due to the surface, linearity should be observed in the $\log J$-V^α (α:constant) plot, at least under one bias polarity for $V \gg k_B T/q$, which is 0.4 mV at 4.5 K. In Figs. 9(b), 9(c), 9(e), and 9(f), the distinct nonlinearity in the Schottky and $\log J$-V^α plots ($\alpha = 1/4-1$) contrasts with the excellent linearity of the J-$V^{1.5}$ plot and the J-V^2-J-V plot of *both the forward- and reverse-bias characteristics*. Therefore, the J-V characteristics in Fig. 9 are incompatible with surface-limited processes. It should be noted that the conventional explanation of J-$V^{1.5}$ such as the ballistic transport (Child-Langmuir law) or spherical geometry[30] is inapplicable to the present experiments.

The shape of the experimental J-V characteristics indicates that the J-V characteristics are consistent with the shallow-trap case of the semianalytical solution with the $n_0 \propto N_t$ [Fig. 9(a)] and constant-n_0 [Fig. 9(d)] approximations. The observation that the sample had metallic T dependence at low T after an extremely intensive injection also suggests

that these traps are shallow. The theoretical J-V characteristics are in excellent agreement with experimental curves over two or three orders of magnitude of the current density. The free parameters for the fittings are two scaling factors (J_{bi2}, V_{bi2}) and the trap-density gradient G because (i) the results are independent of $\Theta(0)$ for $\Theta(0) \ll 1$, (ii) η_k and r_k in Eqs. (4) and (5) are calculated from G, and (iii) $N_t(0)$ appears only in J_{bi2} and V_{bi2} (Appendix C). The expressions for J_{bi2} and V_{bi2} show that an alternative set of parameters can be $n_0(0)\Theta^{-1}(0)L^2/\varepsilon$, $\mu\Theta(0)/L^3$, and $n_0(L)$, where trap free μ is regarded as a material constant.

We examine the numerical consistency of the fitting parameters and compare with the experimental trap-density gradient, which are obtained from another SrTiO$_3$:Cr single crystal exhibiting a small rectification.[9] Assuming $\varepsilon = 10^4 \varepsilon_0$ (ε_0: vacuum permittivity) with trap-free mobility $\mu = 10^4$ cm^2 V^{-1} s^{-1} for SrTiO$_3$ at 4.5K,[51,52] $\Theta(0) = 10^{-9}$ and $n_0/N_t = 10^{-9}$, we obtain $N_t(0) = 1.8 \times 10^{17}$ cm^{-3}, $N_t(L) = 1.8 \times 10^{19}$ cm^{-3}, and $L = 0.065$ μm for Fig. 9(a) and $N_t(0) = 1.6 \times 10^{16}$ cm^{-3}, $N_t(L) = 1.6 \times 10^{19}$ cm^{-3}, and $L = 1.9$ μm for Fig. 9(d). These parameter sets are nonunique: for example, $n_0/N_t = 10^{-8}$, $\Theta(0) = 10^{-6}$, and $L = 0.65$ μm can be another set for Fig. 9(a). These numbers appears in acceptable ranges. In particular, L is regarded as the length of the region having a finite trap-density gradient; the J-V characteristics for trap distributions with and without a constant high-trap-density region or with a valley [Figs. 3(a)–3(d)] are almost the same (Appendix A). Furthermore, the estimated N_t values are favorably compared with the injection-induced in-gap density of state of $(2-8) \times 10^{17}$/cm^3 eV at E_F.[18] X-ray absorption spectroscopy has confirmed the trap-density gradient in a SrTiO$_3$:Cr single crystal showing a small rectification and found that the average G is approximately 3.[9] This number is consistent with the average G of 1.3–3.7, which is the value averaged over the spot size (5×5 μm^2) with use of the above fitting parameters for Fig. 9(a).

The sample of Fig. 10 is a 70-μm-thick BiFeO$_3$ single crystal with 2×2 mm^2 in-plane dimensions with its normal in the direction of one of principal axes of the pseudocubic cell. It has a capacitor structure with ~ 0.6-mm-diameter thick circular Au electrodes on both surfaces. The details of the sample and measurements are described in Ref. 4. Owing to weak BiO chemical bonding, Bi-based ferroelectric oxides contain many traps,[53] especially at the surface, which would yield ohmic contacts. The maximum field of 1 kV/cm used in Fig. 10 may not be sufficiently low to retain the original trap distribution, because the Bi-O bonding is weak and, indeed, the voltages >10 kV/cm are found to markedly change the J-V characteristics. This would explain why the theoretical fitting to one polarity branch is excellent but the fitting to both polarity branches with one fixed set of fitting parameters is less good.

The experimental J-V characteristics in Fig. 10 (open circles) show evident rectification, which resemble that of typical diodes. Choi *et al.*[4] concluded that the observed unidirectionality originated from the bulk part. The theoretical calculation same as those in Sec. VI agree well with the experimental data under both forward and reverse bias. The parameters of the calculation are $G = 75$ and $E_C - E_t = 450$ meV (solid lines) or $G = 100$ and $E_C - E_t = 410$ meV
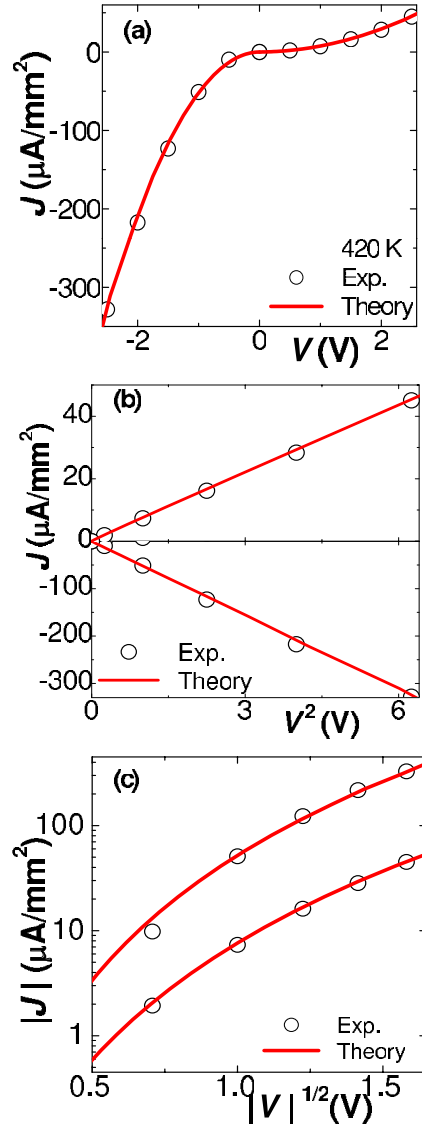
FIG. 11. (Color online) Theoretical (solid lines) and experimental (open circles) J-V characteristics of $In/BaTiO_3/(La,Sr)_2CuO_4/SrTiO_3$ at 420 K in (a) linear, (b) J-V^2, and (c) Schottky plot. This theoretical plot is tentative because the consideration of the effect of the surface may be needed. Two experimental data point at each V, which are overlapped, are those during increasing and decreasing V. The theoretical curves are for $\Theta(0)=0.01$ in the $n_0 \propto N_t$ approximation.

(dashed lines) with $N_t(0)=10^{17}$ cm^{-3}, $N_A^-(x)=0.01N_t(x)$, $N_C=10^{19}$ cm^{-3}, $T=300$ K and two scaling factors.

An additional example is the J-V characteristics of a $BaTiO_3/(La,Sr)_2CuO_4$ film on $SrTiO_3$ single crystal, which has an indium electrode of 0.3 mm^2 area (Fig. 11).[54] The transmission electron microscopy observations showed defects and dislocations asymmetrically distributed along the thickness. The indium/$BaTiO_3$ contact is expected to be nearly ohmic at high T because indium has a low work function and $BaTiO_3$ film is n type. Consequently, the J-V characteristics above 400 K markedly deviate from the surface-limited conduction [Fig. 11(c)]. These observations and the linearity in the $j \propto v^2$ plot [Fig. 11(b)] indicate that the J-V

characteristics are dominated by the bulk-limited conduction. The semianalytical solution for shallow traps provides an excellent fitting with the parameters of $V_{bi2}=0.016$ mV, $J_{bi2}=1.3 \times 10^{-5}$ μA mm^{-2}, and $G=240$.

Another example is the rectifying J-V characteristics of compositionally graded ferroelectric films, which should have a trap-density gradient owing to the structure.[25] By replotting the original data, we find a $j \propto v^{1.6}$ relationship for the forward bias at low voltage and for the reverse bias. These behaviors are inconsistent with the surface-limited conduction but consistent with the present theory. The other example is the J-V characteristics that showed a very small rectification and were originally assigned to a resonant tunneling.[55] By replotting the original data, we find excellent $j \propto v^{1.5}$ relationship below V_{TFL} at all T, which the present theory explains well. Here, J-V characteristics of both tunneling and SCLC ($v > 1$) are T independent or only weakly dependent on T (Fig. 7). Furthermore, by replotting the original data showing the rectifying J-V characteristics of tobacco mosaic virus,[56] we find the $j \propto v^m$ relationship ($m=1.7$–2), which indicates that the present theory can explain the rectification and the PTCR in this system.

The purpose of the study of the $SrTiO_3$ single crystals in Fig. 9 was to clarify whether reversible switching can occur without ferroelectricity or defects because all the previous studies were for thin films of ferroelectrics and paraelectrics[1,5,7,13,14,19] and defects and dislocations are inevitable in thin films. Here, the observation of the polarization (P_S) switching[7] is insufficient to prove that the P_S switching *causes* the resistance switching because we find that the current injection in the ferroelectrics often *accompanies* P_S switching. Because the $SrTiO_3$ crystal are paraelectric above 50 K and exhibit excellent reversible resistance switching with a long retention and a high reproducibility at 300 K,[8] the resistance switching is explicable without P_S.

VIII. CONCLUSION

By regarding the bases of SCLC as generic macroscopic descriptions of bulk drift conduction providing the electrostatic consistency, we formulated the conduction under a trap-density gradient. Both semianalytical and numerical results show bulk-originated unidirectional current flow, i.e., rectification under a trap-density gradient and are in excellent agreement with the experimental J-V characteristics (Figs. 9–11).

The J-V characteristics are ohmic and *bidirectional* at low-level injection, i.e., at $V \ll V_{bi2}$, but exhibit unidirectionality above $V \sim V_{bi2}$ (Figs. 5–8). The major requirements for clear unidirectionality are a large trap-density gradient ($G \gg 1$), a small n_0/n_{t0}, i.e., a small Θ, and a not too large applied voltage of $V > V_{bi2}$. In addition, $N_A^-(x) \propto N_t(x)$ type N_A^- distributions enhance the unidirectionality. The condition for a small Θ is the substantial presence of unionized traps, and for $\Theta \ll 1$, the rectification ratio is independent of Θ. The unidirectional J-V characteristics originating from the difference in V_{TFL} for forward and reverse bias closely resemble those of the standard diodes and are difficult to distinguish from them.

In addition, the trap-density gradient induces a positive-T coefficient of resistance (Figs. 7 and 8) and evident $J \propto V^{1.5}$ characteristics (Figs. 5–8). The $J \propto V^{1.5}$ characteristics appear near $V \sim V_{bi2}$ and are augmented by a heavy compensation, i.e., a large N_A^-/N_t ratio. Therefore, new mechanisms different from original proposals can be possible[25,55,56] (Sec. VII).

The essential difference between the present unidirectionality and the conventional rectification exists in the J-V characteristics at a large V, in particular, $V \gg V_{TFL}$: $J \propto V^2$ and $J \propto \exp(-aV^\alpha/k_B T)$ (a, α: constant), respectively. However, the rigorous proof of this experimental property is usually complicated, because assumption (2) in Sec. III is only satisfied for a small V and a low injection. Indeed, in our experiments, the hysteresis-free J-V characteristics exhibiting rectification show mostly the relationship $J \propto V^m$ ($1 \leq m < 2$, typically $m \sim 1.5$). Here, the absence of J-V hysteresis is the criterion for satisfying assumption (2) and eliminating dielectric relaxation in the J-V characteristics. Nonetheless, the use of a high V can provide *nonrigorous* verification. Numerous J-V characteristics resembling Fig. 8 may have remained unreported because the TFL transition is similar to the breakdown and is often irreproducible.

Electrical detection of the trap-density gradient is possible because of the built-in potential ϕ_{bi}. Equation (1a) is rewritten as $q\phi_{bi} = E_{C0}(x) - E_{C0}(0) = k_B T \ln[n_0(x)/n_0(0)]$. Therefore, Fig. 1(c) indicates the existence of a small ϕ_{bi} ($k_B T \sim 7k_B T$), which should yield a photovoltaic effect under illumination. Indeed, Choi *et al.*[4] reported a photovoltaic effect in the samples used for Fig. 10.

The semianalytical solutions [Eqs. (4)–(7)], which are verified by the numerical solutions, are useful for practical fitting and excellently fit the experimental data. For shallow-trap case, three parameters are required in practice: the scaling factors (V_{bi2}, J_{bi2}) and G. Here, T dependence can be included in the scaling factors. Moreover, *semianalytical solution yields a reasonable fitting even for $k_{max} = 2$ (Appendix A), which substantially facilitates the use of Eqs. (4) and (5).*

Because SCLC is a generic macroscopic description of conduction, it is compatible with elementary processes. Under assumption (2) in Sec III, the high-field characteristics would be outlined by the competition between the TFL transitions and the field dependence of μ. The inclusion of the field dependence of μ into SCLC is studied by Grekov and Sukhorukov for a Pool-Frenkel case[57] and is discussed in Appendix D for a variable range hopping case.

Because an intensive injection changes trap distribution, electric stimulus-induced change in both conduction and rectification is also expected to exist universally. This universality is consistent with the universal existence of the resistance switching in various materials such as metal oxides, nonoxide semiconductors, polymers, and virus (references in Refs. 7 and 8)
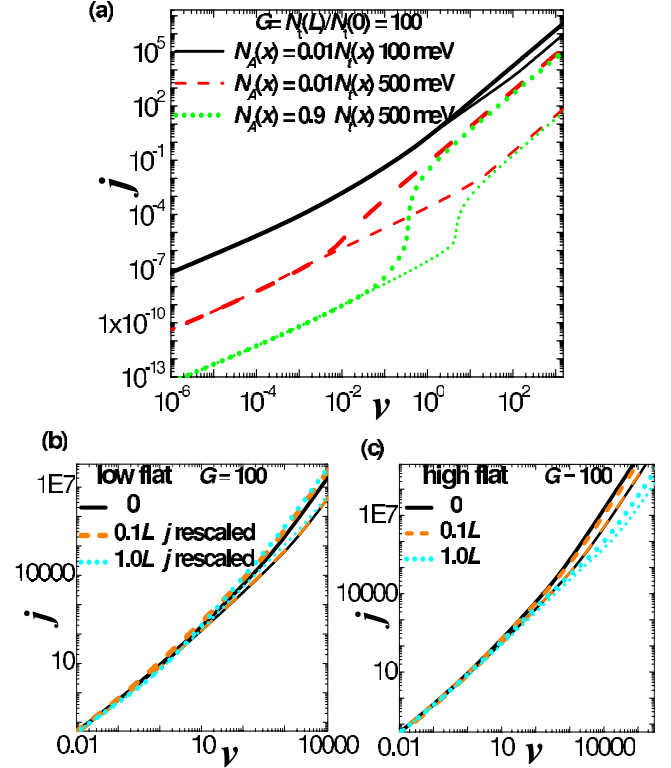
ACKNOWLEDGMENTS

FIG. 12. (Color online) J-V characteristics for variations in N_t distributions, Figs. 3(b)–3(d). (a) Same plots as Fig. 5 for *valley-type trap distributions* [Fig. 3(d)] with the same parameters $[N_t(L)/N_t(0)] = 100$} and the same normalization except for $E_C - E_t = 100$ or 500 meV and $\chi = 0.01$ or 0.9 in $N_A^-(x) = \chi N_t(x)$. [(b) and (c)]: J-V characteristics by semianalytical solution, Eqs. (4) and (5). (b) Solid lines for Fig. 3(a) vs other lines for Fig. 3(b). (c): solid lines for Fig. 3(a) vs other lines for Fig. 3(c). The dashed and dotted lines correspond to the length of the flat region being 10% and 100% of that of the gradient part in Fig. 3(b) or 3(c), respectively. The solid and dashed lines are almost overlapped. The length L used for the normalization of J and V is that of the gradient part. j of the dashed and dotted lines is rescaled by 1.26 and 5.55, respectively, so that the ohmic part is aligned to that for the solid lines.

APPENDIX A: J-V CHARACTERISTICS FOR OTHER TRAP DISTRIBUTIONS

The realistic trap distributions are one of Fig. 3(b)–3(d) but yield essentially the same results as Fig. 3(a). Figure 12(a) is for the valley-type trap distribution, which consists of two exponential distributions, and is calculated numerically similar to Sec. VI. The minimum of N_t is at $x = L/2$, and $N_t(0)$, $N_t(L/2)$, and $N_t(L)$ are 10^{17} cm^{-3}, 10^{15} cm^{-3}, and 10^{19} cm^{-3}, respectively, which gives $N_t(L)/N_t(0) = G = 100$. The parameters except for those in caption are the same as those for Fig. 5. The three J-V characteristics of the valley-type trap distribution in Fig. 12(a) should be compared with those of exponential distributions in Fig. 5 [dashed lines in Fig. 5(a) and solid and dashed lines in Fig. 5(b)]. For the same G, Figs 3(a) and 3(d) yield essentially the same J-V characteristics.

In addition, Figs. 12(b), 12(c), 13(a), and 13(b) are calculated by semianalytical solutions, Eqs. (4) and (5), for
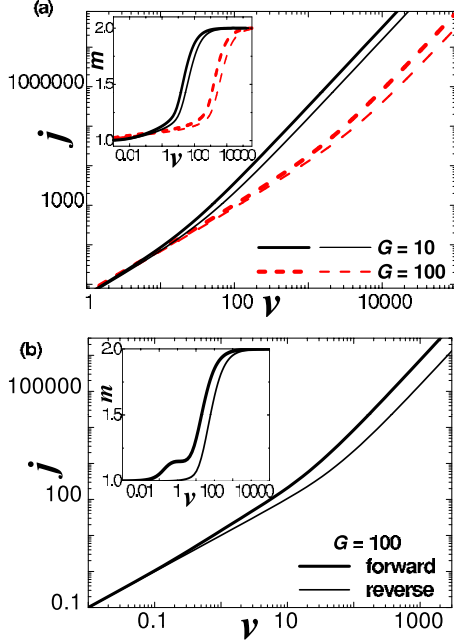
FIG. 13. (Color online) Theoretical J-V characteristics of the forward- and reverse-bias branches for the shallow-trap case calculated by semianalytical solution, Eqs. (4) and (5), for linear and step N_t distribution [Figs. 3(a) and 3(e)]. All the conditions and parameters are the same as those in Fig. 4(a) except for (a) linear N_t distributions and (b) a two-step N_t distribution and constant-n_0 approximation. Insets show the v dependence of m in $j \propto v^m$.

shallow-trap case with $\Theta_0 = 0.01$. The J-V characteristics in Figs. 12(b) and 12(c) are for exponential trap distributions with and without a low- and high-N_t flat region [Figs. 3(a)–3(c)] with $G = 100$, respectively, and are almost the same. The J-V characteristics in Fig. 13 are for linear trap distributions, which are defined by a constant $N_{t,k} - N_{t,k-1}$ in Fig. 3(a), and for an abrupt-step trap distribution [Fig. 3(e), $k_{max} = 2$]. These J-V characteristics are almost the same as those with the same parameters for exponential trap distributions [Fig. 3(a)].

APPENDIX B: CONSTANT-n_0 AND $n_0 \propto N_t$ APPROXIMATION

In the two-level model represented by N_A and N_t, we derive the relationship between n_0 and N_t for graded distribution of *shallow traps* with $\Theta_k < 1$. We first assume that the energy levels of traps are independent of x, which means $N_{A,k}^- \propto N_{t,k}$. To start with, we consider a virtual state where each segment is separated by an infinite distance, and denote the free and trapped carrier density in this state as $\underline{n}_{0,k}$ and $\underline{n}_{t0,k}$, respectively. In this state, the charge neutrality $N_{t0,k}^+ - N_{A,k}^- - \underline{n}_{0,k} = N_{t,k} - N_{A,k}^- - \underline{n}_{0,k}(1 + \Theta_k^{-1}) = 0$ exists in each segment because $\underline{n}_{0,k}/\underline{n}_{t0,k} = n_0(x)/n_{t0}(x) \equiv \Theta_k$. This charge neutrality gives $\underline{n}_{0,k} = g^{-1}N(1 - N_{A,k}^-/N_{t,k})/(1 + \Theta_k)$. Therefore, $\underline{n}_{0,k}$ is constant ($\underline{n}_0$) in the lowest approximation for $\Theta_k \ll 1$ because $N_{A,k}^-/N_{t,k}$ is independent of k. In a higher order of Θ_k, $\underline{n}_{0,k}$ increases with $N_{t,k}$ because $\underline{n}_{0,k} = N_{t,k}g^{-1}N(1 - N_{A,k}^-/N_{t,k})/(g^{-1}N + N_{t,k})$ by $\Theta_k \approx N/gN_{t,k}$.

When all the segments are joined and diffusion starts, the carrier density in the segment with a high $N_{t,k}$ decreases and that in the segment with a low $N_{t,k}$ increases, until ϕ_{bi} is formed. ϕ_{bi} is high at high $N_{t,k}$'s [Fig. 1(c)] because the charge density is positive at high $N_{t,k}$ and negative at low $N_{t,k}$. Consequently, Eq. (1a) shows that $n_0(x)$ in the segment with a high $N_{t,k}$ is higher than that with a low $N_{t,k}$. For $\underline{n}_{0,k} = \underline{n}_0$, $n_0(x) = \underline{n}_0$ also after the diffusion, which is the constant-n_0 approximation and the lowest approximation for $\Theta_k \ll 1$. The next-to-lowest order approximation of $n_0(x)$ is $n_{0,k} = \lambda N_{t,k}$, where λ is a constant (the $n_0 \propto N_t$ approximation). This approximation is sufficient for the present purpose because our main results do not depend on the details of the $n_0(x)$ profile. These results are favorably compared with numerical results in Fig. 2. In addition, positive $n_0 - N_t$ correlations occur by constant $N_{A,k}^-$ and negative $N_{A,k}^- - N_{t,k}$ correlations. Therefore, the situations for the $n_0 \propto N_t$ approximation would widely exist.

The above charge neutrality before diffusion $N_{A,k}^- = N_{t,k} - \underline{n}_{t0,k}(1 + \Theta_k)$ yields $N_{A,k}^- \approx N_{t,k}$ for *shallow traps* with $\Theta_k < 1$ because $\underline{n}_{t0,k} < N_{t,k}$ by Eq. (1b) with $E_{t0} - E_F > k_B T + \ln g$. After the segments are joined and diffusion starts, this quasiequality holds approximately, because $N_{t,k}$ and $N_{A,k}^-$ are unchanged, and $n_{t0,k}$, which changes by diffusion, is a fraction of $N_{t,k}$. For *deep traps*, the same arguments based on infinitely separated segments show that $A_k \propto N_{t,k}$ is an acceptable approximation: the lowest approximation is $n_{0,k} = \underline{n}_0$ and $A_k \equiv N_{t,k}^+/n_{0,k}$ shows $A_k \propto N_{t,k}$.

APPENDIX C: HOW TO FIT DATA AND FACILITATION OF FITTING

The assumption of the injecting ohmic electrodes is only approximately correct. In the two-terminal measurements, the J-V characteristics are given by $V/[R_{C1}(V) + R_B(V) + R_{C2}(V)]$, where R_{C1} and R_{C2} are contact resistances and R_B is the resistance of the bulk part. R_B, R_{C1}, and R_{C2} depend on V. This formula shows that the J-V characteristics are regulated by the dominantly resistive part at given a V range. Because R_{C1} and R_{C2} depend exponentially on V, the regulating part changes critically with V, and the assignment of the regulating part is meaningful only for a given V range.

The fitting procedures are as follows: (1) estimate the exponents (m) under forward and reverse bias of experimental J-V curves and determine the v range. (2) Estimate J_f/J_r at the same $|V|$ of forward and reverse bias. (3) Find an appropriate $N_{t,k\,max}/N_{t,1}$ value by combining this J_f/J_r and the exponents—for a given $N_{t,k\,max}/N_{t,1}$. (4) Finally, scale the theoretical J-V curve so that one point of one of the bias polarities agrees with the experimental J-V curve. Here, abrupt two-step $k_{max} = 2$ distributions [Fig. 3(e)] substantially simplify the calculation and yield J-V curves [Fig. 13(b)] comparable with those with $k_{max} = \infty$ [Fig. 4(a)]. Typical values of the normalizations V_{bi2} and J_{bi2} are

$$V_{bi2} = 18[n_0(0)/10^{11} \text{ cm}^{-3}](L/10^{-5} \text{ cm})^2[10^{-5}/\Theta(0)]/$$

$$[\varepsilon/(100 \times 8.9 \times 10^{-14} \text{ F cm}^{-1})] \text{ (mV)},$$

and

$$J_{bi2} = 46[n_0(0)/10^{11} \text{ cm}^{-3}](\mu/100 \text{ cm}^2 \text{ V}^{-1} \text{ s}^{-1})$$

$$\times (V_{bi2}/18 \text{ mV})/(L/10^{-5} \text{ cm}) \ (\mu\text{A mm}^{-2}).$$

The T dependence of J-V characteristics for shallow-trap case of semianalytical solution is obtained by considering the T dependence of $n_0(0)$ and μ in V_{bi2} and J_{bi2}. Suppose that $n_0(0)$ at $T=T_0$ is obtained from the fitting, then $n_0'(0)$ at $T=T'$ is given by $n_0'(0)=n_0(0)\exp[-\Delta E(T')/T'+\Delta E(T_0)/T_0]$ owing to Eq. (1a), where $\Delta E(T)=[E_{C0}(0)-E_F(T)]/k_B$. Because $V_{bi2} \propto n_0(0)$ and $J_{bi2} \propto n_0^2(0)$, $V \propto \exp[-\Delta E(T')/T']$ and $J \propto \exp[-2\Delta E(T')/T']$. In the lowest approximation, $\Delta E(T)$ is constant.

APPENDIX D: COMPATIBILITY WITH VARIABLE RANGE HOPPING

SCLC and variable range hopping processes can be compatible. Under low electric fields for homogeneous electron distributions, variable range hopping is described by

$$J = 2q^2R^2\nu_{ph}N(E_F)\exp(-2\alpha R - W/k_BT)\mathcal{E}(x), \quad (\text{D1})$$

where R, ν_{ph}, $N(E_F)$, α, and W are hopping distance, hopping frequency related to the phonon spectrum, electron density of states at E_F, decay factor, and energy difference between two states for hopping, respectively.[58]

When the electron distribution $n(x)$ is inhomogeneous, we assume that the electron density near Fermi level $N(E_F)k_BT$ is proportional to $n(x)$, so that J is proportional to $n(x)$. The comparison of Eq. (D1) with $J=qn(x)\mu\mathcal{E}(x)$ indicates that Eq. (D1) is a special case of $J=qn(x)\mu\mathcal{E}(x)$ with μ independent of $\mathcal{E}(x)$. Therefore, the SCLC J-V characteristics are expected. Because Eq. (D1) yields the T dependence $\exp(-X/T^{1/4})$ (X is a constant), this T dependence can coexist with these J-V characteristics of SCLC. At high fields, Eq. (8) changes to $J=\vartheta \exp[-\Gamma/\mathcal{E}^{1/4}(x)]\mathcal{E}(x)$ (ϑ, Γ: constant).[58] Because this V dependence is far sharper than V^2 dependence, we expect that the J-V characteristics follow $\exp[-\Gamma/\mathcal{E}^{1/4}(x)]$, which explains the results by Karg *et al.*[18] The present results were partly published.[59]

[1] S. M. Sze, *Physics of Semiconductor Devices* (Wiley, New York, 1981), Chaps. 2 and 5.

[2] W. W. Zhuang, W. Pan, B. D. Ulrich, J. J. Lee, L. Stecker, A. Burmaster, D. R. Evans, S. T. Tajiri, M. Hsu, A. Shimaoka, K. Inoue, T. Naka, N. Awaya, A. Sakiyama, Y. Wang, S. Q. Liu, N. J. Wu, and A. Ignatiev, Digest of Electron Devices Meeting 2002 (IEDM '02) , p. 193.

[3] A. Beck, J. G. Bednorz, Ch. Gerber, C. Rossel, and D. Widmer, Appl. Phys. Lett. **77**, 139 (2000).

[4] T. Choi, S. Lee, Y. J. Choi, V. Kiryukhin, and S.-W. Cheong, Science **324**, 63 (2009).

[5] S. F. Alvarado, F. La Mattina, and J. G. Bednorz, Appl. Phys. A **89**, 85 (2007).

[6] A. Baikalov, Y. Q. Wang, B. Shen, B. Lorenz, S. Tsui, Y. Y. Sun, Y. Y. Xue, and C. W. Chu, Appl. Phys. Lett. **83**, 957 (2003).

[7] Y. Watanabe, Ferroelectrics **349**, 190 (2007).

[8] Y. Watanabe, J. G. Bednorz, A. Bietsch, Ch. Gerber, D. Widmer, A. Beck, and S. J. Wind, Appl. Phys. Lett. **78**, 3738 (2001).

[9] M. Janousch, G. I. Meijer, U. Staub, B. Delley, S. F. Karg, and B. P. Andreasson, Adv. Mater. **19**, 2232 (2007).

[10] D. S. Shang, Q. Wang, L. D. Chen, R. Dong, X. M. Li, and W. Q. Zhang, Phys. Rev. B **73**, 245427 (2006).

[11] F. La Mattina, J. G. Bednorz, S. F. Alvarado, A. Shengelaya, and H. Keller, Appl. Phys. Lett. **93**, 022102 (2008).

[12] R. Fors, S. I. Khartsev, and A. M. Grishin, Phys. Rev. B **71**, 045305 (2005).

[13] A. Odagawa, H. Sato, I. H. Inoue, H. Akoh, M. Kawasaki, Y. Tokura, T. Kanno, and H. Adachi, Phys. Rev. B **70**, 224403 (2004).

[14] M. Y. Chan, T. Zhang, V. Ho, and P. S. Lee, Microelectron. Eng. **85**, 2420 (2008).

[15] Y. Watanabe, Phys. Rev. B **59**, 11257 (1999).

[16] Y. Watanabe, D. Sawamura, and M. Okano, Appl. Phys. Lett. **72**, 2415 (1998).

[17] N. A. Tulina and I. Y. Borisenko, Phys. Lett. A **372**, 918 (2008).

[18] S. Karg, G. I. Meijer, D. Widmer, and J. G. Bednorz, Appl. Phys. Lett. **89**, 072106 (2006).

[19] D. S. Shang, J. R. Sun, L. Shi, and B. G. Shen, Appl. Phys. Lett. **93**, 102106 (2008).

[20] W. Guan, S. Long, R. Jia, and M. Liu, Appl. Phys. Lett. **91**, 062111 (2007).

[21] Y. Watanabe, Appl. Phys. Lett. **66**, 28 (1995).

[22] Y. Xia, W. He, L. Chen, X. Meng, and Z. Liu, Appl. Phys. Lett. **90**, 022907 (2007).

[23] X. F. Liang, Y. Chen, L. Chen, J. Yin, and Z. G. Liu, Appl. Phys. Lett. **90**, 022508 (2007).

[24] S. Kaku, S. Miyauchi, T. Arai, and Y. Watanabe, Ferroelectrics **370**, 39 (2008).

[25] R. Bouregba, G. Pullain, B. Vilquin, and G. Le Rhun, J. Appl. Phys. **93**, 5583 (2003).

[26] G. T. Wright, Solid-State Electron. **2**, 165 (1961).

[27] L. D. Partain, J. Appl. Phys. **54**, 5218 (1983).

[28] H. Y. Fan, Phys. Rev. **74**, 1505 (1948).

[29] N. F. Mott and R. W. Gurney, *Electronic Processes in Ionic Crystals* (Clarendon Press, Oxford, 1948), Chap. 5.

[30] K. C. Kao and W. Hwang, *Electrical Transport in Solids* (Pergamon, Oxford, 1981), Chaps. 2 and 3.

[31] M. A. Lampert and P. Mark, *Current Injection in Solids* (Academic, New York, 1970), Chaps. 2 and 4.

[32] J. P. Ibbetson and U. K. Mishra, Appl. Phys. Lett. **68**, 3781 (1996).

[33] L.-W. Yin, J. P. Ibbetson, M. M. Hashemi, A. C. Gossard, U. K. Mishra, Y. Hwang, T. Zhang, and R. M. Kolbas, Appl. Phys. Lett. **60**, 2005 (1992).

[34] F. Neumann, Y. A. Genenko, C. Melzer, S. V. Yampolskii, and H. von Seggern, Phys. Rev. B **75**, 205322 (2007).

[35] R. W. I. de Boer and A. F. Morpurgo, Phys. Rev. B **72**, 073207(2005).

[36] E. Tutiš, M. Bussac, B. Masenelli, M. Carrard, and L. Zuppiroli, J. Appl. Phys. **89**, 430 (2001).

[37] W. Chandra, L. K. Ang, K. L. Pey, and C. M. Ng, Appl. Phys. Lett. **90**, 153505 (2007).

[38] M.-A. Nicolet, J. Appl. Phys. **37**, 4224 (1966).

[39] Y. K. Sharma, J. Appl. Phys. **50**, 5381 (1979).

[40] A. Pitarch, G. Garcia-Belmonte, and J. Bisquert, Proc. SPIE **5519**, 304 (2004).

[41] J. Sworakowski, J. Appl. Phys. **41**, 292 (1970).

[42] N. Koda, Jpn. J. Appl. Phys., Part 1 **25**, 200 (1986).

[43] G. W. Bąk and A. Lipiński, Thin Solid Films **238**, 290 (1994).

[44] P. K. Larsen and R. Metselaar, Phys. Rev. B **8**, 2016 (1973).

[45] A. G. Milnes and D. L. Feucht, *Heterojunctions and Metal Semiconductor Junctions* (Academic Press, New York, 1972).

[46] D. J. DiMaria and J. W. Stasiak, J. Appl. Phys. **65**, 2342 (1989).

[47] C. M. Osburn and E. J. Weitzman, J. Electrochem. Soc. **119**, 603 (1972).

[48] R. H. Walden and R. J. Strain, Proceedings of the Eighth Annual Reliability Physics Symposium, Las Vegas, Nevada, USA, 1970 (IEEE, New York, 1971), p. 23.

[49] I.-C. Chen, S. E. Holland, and C. Hu, IEEE Trans. Electron Devices **32**, 413 (1985).

[50] P. E. Blöchl and J. H. Stathis, Phys. Rev. Lett. **83**, 372 (1999).

[51] M. Ahrens, R. Merkle, B. Rahmati, and J. Maier, Physica B **393**, 239 (2007).

[52] R. Moos and K. H. Härdtl, J. Appl. Phys. **80**, 393 (1996).

[53] Y. Watanabe, Y. Matsumoto, and M. Tanamura, Jpn. J. Appl. Phys., Part 1 **35**, 5745 (1996).

[54] S. Kaku and Y. Watanabe (unpublished).

[55] J. Son and S. Stemmer, Phys. Rev. B **80**, 035105 (2009).

[56] R. J. Tseng, C. Tsai, L. Ma, J. Ouyang, C. S. Ozkan, and Y. Yang, Nat. Nanotechnol. **1**, 72 (2006).

[57] E. V. Grekov and O. G. Sukhorukov, Phys. Status Solidi B **165**, 219 (1991).

[58] N. F. Mott and E. A. Davis, *Electronic Processes in Noncrystalline Materials*, 2nd ed. (Clarendon, Oxford, 1979).

[59] Y. Watanabe, J. Phys. Soc. Jpn. **78**, 104712 (2009); Bull. Am. Phys. Soc. **54** (1), 1053 (2009) (March Meeting 2009 Z10-3).